Systems/Circuits

Development of Intrinsic Connectivity in the Central Nucleus of the Mouse Inferior Colliculus

Joshua Sturm,[1,2,4] Tuan Nguyen,[5] and Karl Kandler[1,2,3]

[1]Department of Otolaryngology and [2]Department of Neurobiology, University of Pittsburgh School of Medicine, Eye and Ear Institute, Pittsburgh, Pennsylvania 15213, [3]Center for the Neural Basis of Cognition, University of Pittsburgh, Pittsburgh, Pennsylvania 15213, [4]Medical Scientist Training Program, University of Pittsburgh School of Medicine, Pittsburgh, Pennsylvania 15261, and [5]College of New Jersey, Ewing, New Jersey 08628

The inferior colliculus (IC) in the mammalian midbrain is the major subcortical auditory integration center receiving ascending inputs from almost all auditory brainstem nuclei as well as descending inputs from the thalamus and cortex. In addition to these extrinsic inputs, the IC also contains a dense network of local, intracollicular connections, which are thought to provide gain control and contribute to the selectivity for complex acoustic features. However, in contrast to the organization of extrinsic IC afferents, the development and functional organization of intrinsic connections in the IC has remained poorly understood. Here we used laser-scanning photostimulation with caged glutamate to characterize the spatial distribution and strength of local synaptic connections in the central nucleus of the inferior colliculus of newborn mice until after hearing onset (P2-P22). We demonstrate the presence of an extensive excitatory and inhibitory intracollicular network already at P2. Excitatory and inhibitory synaptic maps to individual IC neurons formed continuous maps that largely overlapped with each other and that were aligned with the presumed isofrequency axis of the central nucleus of the IC. Although this characteristic organization was present throughout the first three postnatal weeks, the size of input maps was developmentally regulated as input maps underwent an expansion during the first week that was followed by a dramatic refinement after hearing onset. These changes occurred in parallel for excitatory and inhibitory input maps. However, the functional elimination of intrinsic connections was greater for excitatory than for inhibitory connections, resulting in a predominance of intrinsic inhibition after hearing onset.

Key words: **auditory; photostimulation; synaptic circuit; uncaging**

Introduction

The inferior colliculus (IC) in the midbrain is the major subcortical auditory integration center. It receives ascending inputs from almost all auditory brainstem nuclei, descending inputs from the thalamus and cortex, and intracollicular projections from the contralateral inferior colliculus (Adams, 1979, 1980; Saldaña and Merchán, 1992; Saldaña et al., 1996; Winer et al., 1998; Malmierca, 2004; Malmierca et al., 2005). In the central nucleus of the IC (CNIC), afferent projections terminate in a tonotopic manner with ascending brainstem projections aligning to anatomically defined fibrodendritic laminae (Morest and Oliver, 1984; Oliver and Morest, 1984; Stiebler and Ehret, 1985; Malmierca et al., 1993; Gabriele et al., 2000a, 2007; Henkel et al., 2005; Miller et al., 2005; Henkel et al., 2007).

In addition to the wide array of ascending and descending projections, the CNIC also contains a dense network of local, intrinsic connections (Oliver et al., 1991; Saldaña and Merchán, 1992; Casseday et al., 2002; Fathke and Gabriele, 2009; Wallace et al., 2013). Local networks are thought to give rise to the majority of synapses in the IC (Saldaña and Merchán, 2005), suggesting that intrinsic connections significantly contribute to the response properties of IC neurons. However, while the organization and integration of extrinsic projections to the IC are becoming increasingly well understood (Brunso-Bechtold et al., 1981; Maffi and Aitkin, 1987; Oliver, 1987, 2000; Faingold et al., 1993; Burger and Pollak, 2001; Malmierca et al., 2002, 2005; Henkel et al., 2005; Cant and Benson, 2008; Pollak et al., 2011), the anatomical and functional organization of intrinsic connections in the CNIC has remained largely obscure.

Intrinsic axons arise from disc-shaped (flat) as well as stellate (less flat) cells, the two major morphological cell types in the CNIC (Oliver and Morest, 1984; Meininger et al., 1986; Oliver et al., 1991; Malmierca et al., 1993; Wallace et al., 2012). Because both disc-shaped and stellate cells can be glutamatergic or GABAergic (Oliver et al., 1994; Ono et al., 2005), intrinsic connections likely are excitatory as well as inhibitory. Local axon collaterals from disc-shaped cells predominantly project along the same fibrodendritic laminae as the dendrites of their parent neurons (Oliver et al., 1991), and intralaminar local axons likely

Received June 4, 2014; revised Sept. 22, 2014; accepted Sept. 26, 2014.

Author contributions: J.S., T.N., and K.K. designed research; J.S. and T.N. performed research; T.N. contributed unpublished reagents/analytic tools; J.S., T.N., and K.K. analyzed data; J.S., T.N., and K.K. wrote the paper.

This work was supported by National Institute on Deafness and Other Communication Disorders Grant 04199 to K.K., Grant 1F30DC014177 to J.S., and Grant T32 GM08208-22 to J.S. We thank Xinyan Gu for technical support, Drs. Gunsoo Kim and Anna Magnusson for comments on a previous version of the manuscript, and the Auditory Research Group for discussions.

The authors declare no competing financial interests.

Correspondence should be addressed to Dr. Karl Kandler, Department of Otolaryngology, University of Pittsburgh School of Medicine, Biomedical Science Tower 3, 3501 Fifth Avenue, Pittsburgh, PA 15261. E-mail: kkarl@pitt.edu.

DOI:10.1523/JNEUROSCI.2276-14.2014

 0270-6474/14/3415032-15$15.00/0

connect IC neurons that are tuned to similar sound frequencies but may reside in different functional zones (Brunso-Bechtold et al., 1981; Maffi and Aitkin, 1987; Shneiderman and Henkel, 1987; Oliver, 2005; Cant and Benson, 2006; Loftus et al., 2010). In contrast, local axons from stellate cells can spread significantly beyond a fibrodendritic laminae (Oliver et al., 1991), thus potentially connecting neurons that are tuned to different sound frequencies (Merzenich and Reid, 1974; Ehret and Romand, 1994; Schreiner and Langner, 1997; Malmierca et al., 2008).

The contribution of intrinsic connections to an IC neuron's response properties is poorly understood. Recent evidence indicates that intrinsic connections are activated at higher sound intensities than extrinsic inputs (Grimsley et al., 2013). The recruitment of intrinsic networks increases the dynamic range of IC neurons but has little effect on their frequency or intensity tuning. Activation of intrinsic networks at higher sound levels may also contribute to the intensity-dependent dynamic nature of the spectrotemporal receptive fields of IC neurons (Lesica and Grothe, 2008).

To better understand the functional organization and the development of the intrinsic networks in the CNIC, we used laser-scanning photostimulation in brain slices from developing mice to characterize the strength and the spatial distribution of local excitatory and inhibitory inputs and their developmental refinement.

Materials and Methods

Animals and slice preparation

Experimental procedures were performed in accordance with National Institutes of Health guidelines and were approved by the Institutional Animal Care and Use Committee at the University of Pittsburgh. Brain slices were prepared from neonatal CBA/CaJ mice of either sex (The Jackson Laboratory) that ranged in age from postnatal day 2 (P2) to P22. For brain slice preparation, animals were deeply anesthetized with isofluorane, decapitated, and their brains were immediately removed. Coronal midbrain slices (300 μm) were then prepared using a vibrating microtome. Cuts were in an ~30 degree angle in a dorsocaudal to ventrorostral direction. Consistency of this angle was verified using anatomical landmarks in the slice (IC slice contained fibers of the lateral lemniscus that entered the IC; slice contained ventral areas just rostral to the lateral superior olive). Slices were incubated for 30 min at 34°C in ACSF (composition in mM as follows: 1.3 $7H_2O \times MgSO_4$, 124 NaCl, 5 KCl, 10 dextrose, 1.25 KH_2P0_4, 26 $NaHCO_3$, 2.0 CaCl) followed by 1–3 h incubation at 22°C-25°C (Kim and Kandler, 2003). The synaptic inputs of 89 neurons in the CNIC from 59 mice were mapped. These mice were grouped into four age ranges: P2-P4 (11 animals, 19 neurons), P7-P9 (18 animals, 21 neurons), P13-P15 (23 animals, 29 neurons), and P19-P22 (7 animals, 20 neurons).

Electrophysiological recordings

Whole-cell recordings were aimed at the CNIC using the inferred demarcations of the lateral and dorsal cortices of the IC, which, in most cases, were visible in our slices. Although the CNIC was clearly recognizable within these defined borders at all ages, individual CNIC neurons cannot be unequivocally distinguished from neurons in the external cortices based on 2D dendritic morphology alone. Thus, to minimize the probability of incorrectly selecting neurons from outside the CNIC, slices that contained the caudal part of the IC (first slice containing the IC in our caudal to rostral series) or that contained the caudal part of the superior colliculus were excluded. Using this procedure, we only recorded from one slice per animal (the second 300 μm slice) and in which we only targeted neurons from within the center of the CNIC. Recordings were performed in a submersion-type chamber (3–4 ml/min perfusion with oxygenated ACSF at 22°C–25°C) mounted on an upright microscope (Zeiss AxioExaminer A1). Borosilicate glass pipettes (5–7 MΩ) were filled with a cesium-based internal solution containing (composition in mM as follows: 110 D-gluconic acid ($C_6H_{12}O_7$), 120 $CsOH \times H_2O$, 11 EGTA, 1 $MgCl_2 \times 6H_2O$, 1 $CaCl_2 \times 2H_2O$, 10 HEPES, 0.3 GTP disodium salt, 2.0 ATP disodium salt, 5 QX314-Cl $\times$ H_2O and 0.5% biocytin, pH 7.2, 314 mOsm/L). Whole-cell currents in voltage-clamp mode were acquired with a Multiclamp 700B amplifier (Molecular Devices) and a Digidata-1440A A/D converter (Molecular Devices) at a sampling rate of 10 KHz using pClamp 10 software (Molecular Devices). Voltages were corrected for a junction potential of −13 mV. All pharmacological drugs were bath applied.

Synaptic input mapping

The spatial distribution of presynaptic inputs to CNIC neurons was determined using focal photolysis of *p*-hydroxyphenacyl-glutamate (0.1 mM, MNI glutamate, Tocris Bioscience). A custom-built system was used to guide the size, location, and duration of the UV light spot used to photolyze MNI-glutamate. A UV laser (DPSS Laser, 3510-30, 2 W) was used as a light source, and placement of the uncaging spot was steered with galvanometers (Cambridge Technology, 6210H). Uncaging position, electrophysiological data acquisition, and analysis were under the control of custom-written Labview-programs linked to pClamp software (written by Tuan Nguyen).

Input maps were only collected if cells had a holding current <100 pA and access resistance <50 mΩ. UV light pulses (355 nm) were delivered at 1 Hz in a random order. Light intensity was 2 mW (measured at slice position), light duration was 1 ms, and UV spot size on the slice was 20 μm. For mapping, 5 mM QX314 (Tocris Bioscience) was included in the internal solution to prevent spiking at positive holding potentials. An initial map of the entire IC was collected first with stimulation targets spaced 80 μm apart (see Fig. 1*B*). Responsive areas were then mapped at a finer resolution with stimulation sites spaced 40 μm apart (see Fig. 1*B*).

Excitatory and inhibitory synaptic responses were isolated by holding cells at −65 and 0 mV, respectively (see Fig. 1*C*). For each condition, 3 input maps were obtained successively and the average map was used for analysis (see Fig. 1*D*). To distinguish synaptic responses from direct stimulation of the recorded cell, input mapping was repeated in the presence of 1 μM TTX (Alomone Labs) (see Fig. 1*D*). In the few cases in which maps with TTX could not be obtained, responses elicited close to the recorded neuron were classified as synaptic if their onset latency was >7 ms. In these cases, choosing this conservative value may miss short-latency synaptic responses arising from locations very close to the recorded cell. When input maps were obtained in the absence and presence of TTX, similar maps were obtained using either onset latencies or TTX sensitivity as criteria.

Excitability mapping

Excitability mapping experiments were performed with loose-seal patches (20–40 MΩ) using patch pipettes (5–10 MΩ) filled with ACSF. After forming a loose seal, UV light was delivered in a 20 μm grid (225 stimulation sites delivered at random locations) surrounding the recording. For each cell, three consecutive excitability maps were obtained, and the average number of spikes per stimulation site was used to create excitability maps.

Data analysis

Input map shape. Elliptical functions of best fit (least-squares fit, ImageJ, National Institutes of Health) were assigned to individual excitatory and inhibitory input maps. An "ellipticity factor" (ratio of minor axis, m; to major axis, M), was then calculated for each map (see Fig. 4*B*). Ellipticity factor values that approach 1 describe input maps that were circular, whereas decreasing ellipticity factor values describe input maps that were increasingly elliptical. The angle of the long axis to the horizontal (lateral-to-medial) axis was determined with ImageJ software.

Synaptic input area. Synaptic input area was determined by subtracting the responsive uncaging area obtained in TTX (direct response area) from the total input map. To account for the expansion of the IC size during development, synaptic input areas were normalized to the cross-sectional IC area for each age group (see Fig. 5*Bi–iii*).

Synaptic input strength. Total excitatory and inhibitory synaptic strengths were calculated as the sums of the synaptic charge (pC) elicited from all stimulation sites at holding potentials of −65 and 0 mV, respectively.

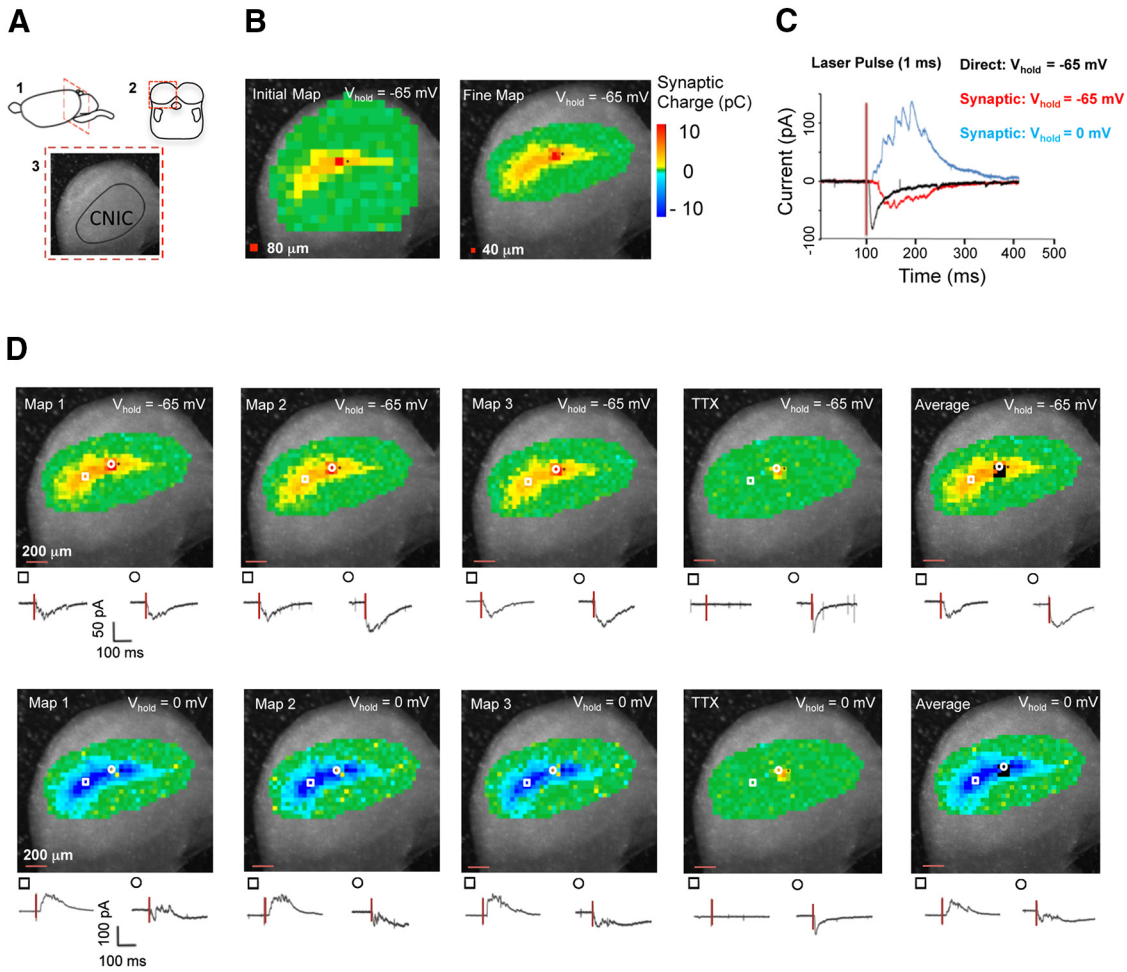

Figure 1. Mapping local inputs in the CNIC using laser scanning photostimulation. ***A***, Coronal brain slices (300 μm) containing the CNIC were prepared from P2–P15 mice. ***B***, An initial, low-resolution input map of the entire IC is first generated by spacing stimulation sites 80 μm apart. Responsive areas are then rescanned at a finer resolution with a stimulation site spacing of 40 μm. ***C***, Excitatory (red trace) and inhibitory (blue trace) synaptic inputs are distinguished by holding neurons at −65 and 0 mV, respectively. Direct activation of the recorded cell by uncaged glutamate elicits short latency, direct responses. ***D***, Example of three consecutively obtained excitatory (top row) and inhibitory (bottom row) synaptic input maps (P8). TTX (1 μM) abolishes synaptic responses but leaves direct responses intact. Example current traces of synaptic (square) and direct (circle) responses are shown for each map. Red lines indicate laser pulse. Maps 1–3 were used to created average input in which sites with direct responses are marked in black.

Statistical analysis

Data are presented as mean ± SEM. Data were tested for normal distribution, and both unpaired *t* tests (two-tailed) and Mann–Whitney tests were used to determine statistical significance of differences between groups (GraphPad Prism). Statistical significance was set to $p < 0.05$.

Results

Spatial mapping of local synaptic inputs to single CNIC neurons

To map the organization of intrinsic excitatory and inhibitory synaptic networks in the developing CNIC, we used whole-cell patch-clamp recordings with laser-scanning photostimulation. For each neuron, we first scanned the entire CNIC at a resolution of 80 μm to identify the overall layout of presynaptic sites. We then obtained finer-scale maps at a resolution of 40 μm from the regions that contained responsive stimulation sites (Fig. 1*B*). To distinguish between excitatory and inhibitory synaptic responses, maps were obtained while holding the membrane potential of the recorded neurons at −65 mV, the reversal potential for chloride, to isolate excitatory responses, and at 0 mV, near the reversal potential of glutamatergic responses, to isolate inhibitory responses (Fig. 1*C*). Both excitatory and inhibitory input maps were highly reproducible in successive iterations and the average map from three iterations was used for all further analysis (Fig. 1*D*). Synaptically elicited responses were distinguished from responses to direct glutamate stimulation of the recorded cell (direct responses) by their onset latencies (>7 ms) (Fig. 1*C*) and their sensitivity to the voltage-gated sodium channel blocker TTX (1 μM) (Fig. 1*D*). Areas from which direct responses were elicited were excluded from the analysis of input maps (Fig. 1*D*).

Consistent with previous anatomical studies showing the absence of glycinergic neurons in the IC (Oliver et al., 1994; Ito et al., 2009), all inhibitory responses were abolished by the $GABA_A$-receptor antagonist gabazine (GBZ, 5 μM, $n = 6$ neurons, $p = 0.001$, Mann–Whitney test) (Fig. 2*B*). In contrast, GBZ had no effect on excitatory synaptic currents or on excitatory input maps ($n = 6$, $p = 0.741$, Mann–Whitney test) (Fig. 2*A*,*C*).

Input maps represent monosynaptic connections

Previous studies have shown that disinhibiting the IC favors the recruitment of polysynaptic circuits, leading to an increase in the duration of synaptic responses and response areas (Moore et al., 1998; Sivaramakrishnan and Oliver, 2006; Chandrasekaran et al., 2013). In our mapping experiments, GBZ did not change excitatory input maps (Fig. 2*C*), suggesting that our low-intensity

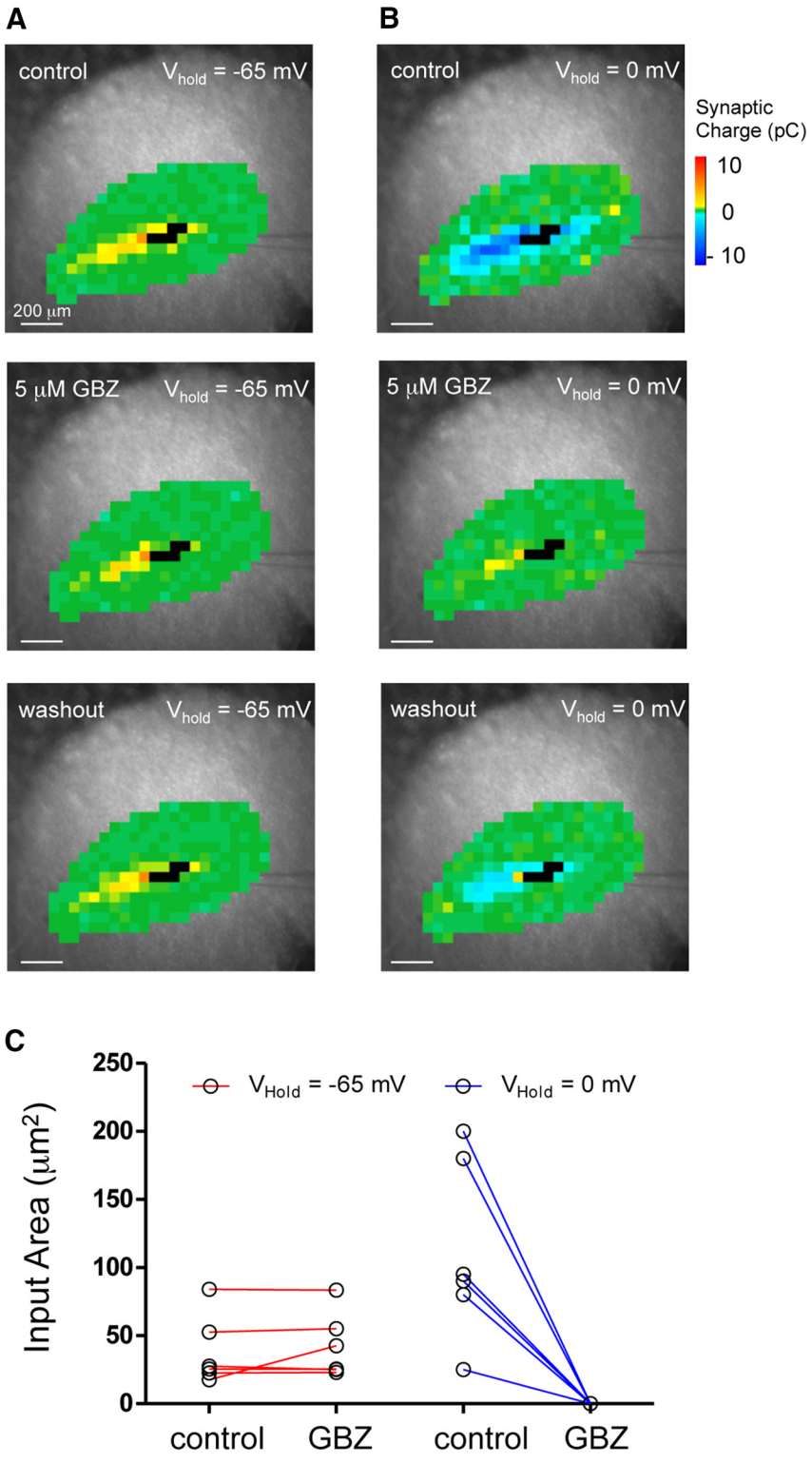

Figure 2. Intracollicular inhibitory connections are mediated by GABA. For a subset of neurons ($n = 6$), 5 μM GBZ was bath-applied during input mapping. ***A***, Excitatory synaptic input maps for a CNIC neuron (P8) before, during, and after washout of 5 μM GBZ. ***B***, Inhibitory synaptic input maps from the same neuron shown in ***A***. Direct response areas are marked in black. ***C***, Size of excitatory (red) and inhibitory (blue) input areas from 6 neurons before (control) and after application of GBZ (+ GBZ). Inhibitory map size was calculated exclusively based on outward currents at 0 mV.

uncaging conditions (0.1 mM caged glutamate and 2 mW of laser power) primarily activated monosynaptic connections, which are not affected by disinhibition. This assumption is further supported by the onset latencies of synaptic currents. First, there was no difference in the latencies of excitatory versus inhibitory responses (Fig. 3*C*,*D*), which, however, would be expected if a significant fraction of inhibitory responses were caused by the activation of disynaptic connections. Second, onset latencies increased smoothly with increasing stimulation distance at similar rates for excitatory ($r^2 = 0.97$, slope = 34.4 ms/mm) and inhibitory responses ($r^2 = 0.926$, slope = 36.4 ms/mm, $Slope_{Inhibitory}$ vs $Slope_{Excitatory}$, $p = 0.209$, ANCOVA) (Fig. 3*B*), and these rates were similar to those reported for uncaging-activated monosynaptic connections in the cochlear nucleus (Campagnola and Manis, 2014). Finally, if monosynaptic connections are strong enough to generate spikes in postsynaptic neurons, one would expect that neurons close to the recorded cell contribute to the excitability maps, resulting in excitability maps that are larger than direct response areas. This was not the case, however, as the average size of direct response areas (in the presence of TTX) was very similar to the area over which photostimulation generated spikes in cell-attached mode (without TTX, excitability area) (direct response area = 20,890 ± 1643 μm^2, $n = 68$ cells; excitability area = 19,840 ± 5020 μm^2, $n = 17$ cells; direct vs excitability, $p = 0.11$, Mann–Whitney test). Thus, single stimuli do not elicit synaptically generated spikes in the recorded neuron, which means that unitary connections in the IC are weak, requiring the activity of several to many connections to elicit the postsynaptic neuron to spike. Together, these results suggest that the excitatory and inhibitory input maps obtained with our conditions primarily reflect monosynaptic connections.

Spatial organization of excitatory and inhibitory synaptic intrinsic inputs

At all ages examined, intrinsic input maps were elongated and oriented along the ventrolateral to dorsomedial direction, the presumed isofrequency contour of the CNIC (Willott and Shnerson, 1978; Romand and Ehret, 1985; Romand and Ehret, 1990). The angle of the isofrequency axis in the coronal plane of the mouse IC shortly after hearing onset is ~35°–55° (Romand and Ehret, 1990). In each of our age groups, the average orientation angles of both excitatory and inhibitory input maps (determined from the fitted ellipses) fell in that range (excitatory maps: P2-P4 = 43.8 ± 4.2°, $n = 18$; P7-P9 = 37.4 ± 3.0°, $n = 20$; P13-P15 = 53.1 ± 7.0°, $n = 15$; P19-P22 = 45.1 ± 11°, $n = 9$; inhibitory maps: P2-P4 = 38.1 ± 4.2°, $n = 13$; P7-P9 = 35.7 ± 3.0°, $n = 20$; P13-P15 = 47.1 ± 4.3°, $n = 14$; P19-P22 = 38.2 ± 10°, $n = 9$; excitatory vs inhibitory, $p = 0.577$, Mann–Whitney test).

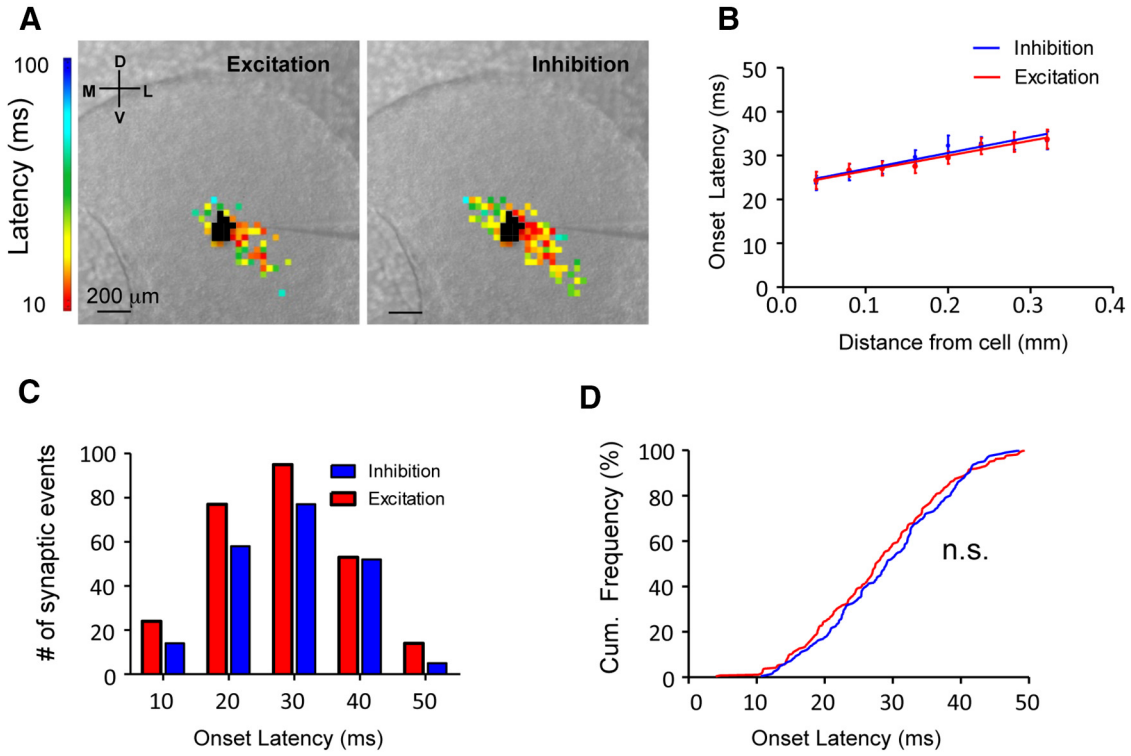

Figure 3. Synaptic response latencies are similar for excitatory and inhibitory responses. ***A***, Example of an excitatory and inhibitory synaptic input maps color-coded by onset latency (from a P8 mouse). Black squares represent stimulation sites that elicited direct responses. ***B***, Mean synaptic onset latencies plotted as a function of distance from the recorded cell. Lines are least-squares regression fits for excitation (red, $r^2 = 0.97$, slope = 34.4 ms/mm) and inhibition (blue, $r^2 = 0.926$, slope = 36.4 ms/mm). Error bars indicate SEM. ***C***, Frequency histogram of onset latencies of excitatory (red) and inhibitory (blue) synaptic responses ($n = 5$ cells). ***D***, Cumulative frequency distributions of excitatory (red line) and inhibitory (blue line) synaptic onset latencies (Kolmogorov–Smirnov, $p = 0.192$). n.s., Not significant.

To quantify the shape of input maps, we fit input maps with an ellipse and calculated the "ellipticity factor" (EF, ratio of minor to major axis; referred to elsewhere as the "compressibility factor," see Maling, 1993) (Fig. 4*B*). At all ages, EFs for excitatory and as well as inhibitory input maps were 0.5, indicating that input maps were elongated, stretching twice as long along the isofrequency direction than along the tonotopic axis (Fig. 4*C*). The degree of elongation changed during the first three postnatal weeks, such that excitatory maps became more elongated during the first postnatal week (excitatory, $EF_{P2\text{-}P4} = 0.53 \pm 0.14$, $n = 18$; $EF_{P7\text{-}P9} = 0.44 \pm 0.16$, $n = 20$; $p < 0.05$, Student's t test), reversed to a more circular shape during the second postnatal week ($EF_{P13\text{-}P15} = 0.58 \pm 0.20$, $n = 17$; $p < 0.001$, Student's t test), and then became more elongated again during the third postnatal week ($EF_{P19\text{-}P22} = 0.44 \pm 0.05$, $n = 9$; $p < 0.05$, Student's t test). Inhibitory maps underwent parallel changes during this period (inhibitory, $EF_{P2\text{-}P4} = 0.52 \pm 0.17$, $n = 13$; $EF_{P7\text{-}P9} = 0.39 \pm 0.09$, $n = 20$; $EF_{P13\text{-}P15} = 0.60 \pm 0.19$, $n = 17$; $EF_{P19\text{-}P22} = 0.45 \pm 0.05$, $n = 10$; P2-P4 vs P7-P9, $p < 0.05$, Student's t test; P7-P9 vs P13-P15, $p < 0.01$, Student's t test; P13-P15 vs P19-P22, $p < 0.05$, Student's t test) (Fig. 4*C*). At each age group, excitatory input maps were clustered into two distinct populations, which differed in their EF values (P2-P4, $r^2 = 0.98$, sum of 2 Gaussian fits; P7-P9, $r^2 = 0.98$, sum of 2 Gaussian fits; P13-P15 $r^2 = 0.89$, sum of 2 Gaussian fits; P19-P22, $r^2 = 89$, sum of 2 Gaussian fits) (Fig. 4*Di–iv*). No separation into two populations was evident at any age for inhibitory input maps.

Developmental refinement of excitatory and inhibitory intrinsic input maps

The size of both excitatory and inhibitory input maps changed during development, expanding during the first postnatal week and retracting during the second and third weeks (Fig. 5*A*,*Bi*). To account for the growth of the IC during this period (Fig. 5*Bii*), we normalized input areas to the cross-sectional areas of the IC (Fig. 5*Biii*). Between P2-P4 and P7-P9, the normalized size of excitatory and inhibitory input maps significantly increased (Fig. 5*B*,*C*). Excitatory maps increased by ~87% (from 0.14 to 0.26, $n = 39$; $p = 0.01$, Student's t test) and inhibitory input maps increased by 63.0% (0.17 to 0.28, $n = 34$; $p = 0.01$, Student's t test). This initial map growth was followed by a significant shrinkage of input maps during the second postnatal week. Between P7-P9 and P13-P15, excitatory input area decreased by ~70% (from 0.26 to 0.08, $n = 49$; $p < 0.001$, Student's t test), and inhibitory input area decreased by 55% (from 0.28 to 0.12, $n = 46$; $p < 0.001$, Student's t test) (Fig. 5*B*,*C*). In addition, although input maps were present in virtually all neurons before hearing onset, input maps were observed in only 69% of cells (20 of 29) immediately after hearing onset. Map refinement continued during the third postnatal week. Between P13-P15 and P19-P22, excitatory input area decreased by 70% (from 0.08 to 0.02, $n = 36$; $p < 0.01$, Mann–Whitney test), and inhibitory input area decreased by ~37%, but this decrease was not statistical significant (from 0.12 to 0.07, $n = 36$, $p = 0.21$, Student's t test) (Fig. 5*B*,*C*). Similar to the P13-P15 age range, input maps were observed in only 70% of cells between P19-P22 (14 of 20).

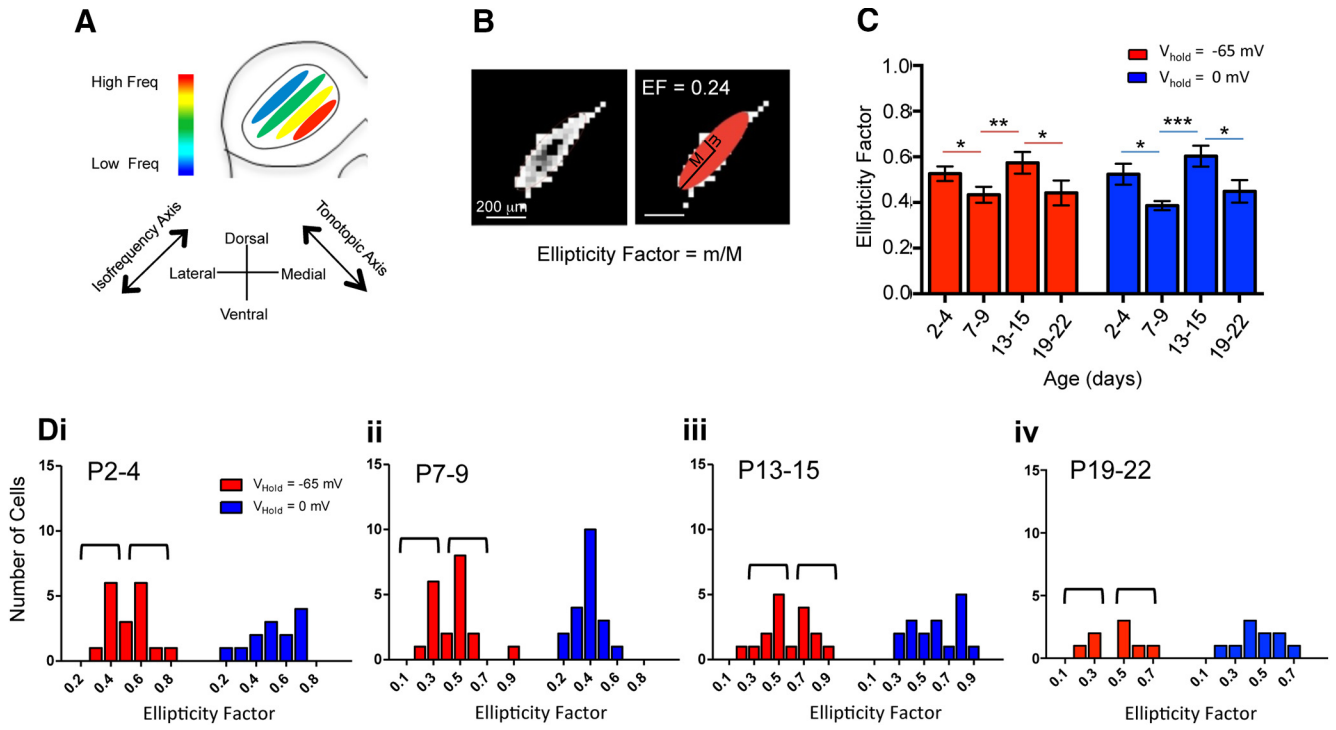

Figure 4. Excitatory and inhibitory synaptic input maps are oriented along the isofrequency axis. ***A***, Schematic illustration of "isofrequency laminae" in the left CNIC. ***B***, Example of an excitatory synaptic input map (left) fitted with an elliptical function (filled red). ***C***, Developmental changes of ellipticity factors for excitatory (red) and inhibitory (blue) input maps. Error bars indicate SEM. *$p < 0.05$ (two-tailed *t* test). **$p < 0.01$ (two-tailed *t* test). ***$p < 0.001$ (two-tailed *t* test). ***D***, Histogram of ellipticity factors for excitatory (red) and inhibitory (blue) input maps at P2-P4 (***i***), P7-P9 (***ii***), P13-P15 (***iii***), and P19-P22 (***iv***). Black brackets represent distinct populations of excitatory input map shapes.

To control for possible age-dependent changes in the effectiveness by which uncaged glutamate elicits action potentials in CNIC neurons, which could influence the size of input maps, we used cell-attached recordings to construct excitability maps (Fig. 5*D*). In all age groups, glutamate uncaging over the recorded cell elicited an average of 2–3 action potentials per stimulation (Fig. 5*E*). Thus, the changes in the sizes of input maps reflect the formation of new functional intrinsic connections during the first postnatal week followed by the silencing and/or elimination of connections during the end of the second postnatal week.

To determine whether the addition and elimination of synaptic inputs was biased toward either the isofrequency or the tonotopic axis, we quantified the amount of map changes along the ventrolateral (VL) to dorsomedial (DM) direction (isofrequency axis) and along the ventromedial (VM) to dorsolateral (DL) direction (tonotopic axis) (Fig. 6*A*,*B*). For the P13-P15 and P19-P22 age groups, this analysis was restricted to those neurons that received input maps exceeding 1% of the IC area (31 of 49 neurons). Between P2-P4 and P7-P9, excitatory as well as inhibitory input maps extended along the isofrequency axis, with similar magnitudes toward the VL (excitatory, $p < 0.001$, $n = 20$; inhibitory, $p < 0.01$, $n = 20$) and the DM directions (excitatory, $p < 0.05$, $n = 20$; inhibitory, $p < 0.05$, $n = 20$) (Fig. 6*C*). In contrast, neither the excitatory nor the inhibitory maps extended along the tonotopic axis (DL direction: excitatory, $p = 0.33$, $n = 20$; inhibitory, $p = 0.64$, $n = 20$: VM direction: excitatory, $p = 0.09$, $n = 20$; inhibitory, $p = 0.11$, $n = 20$).

Between P7-P9 and P13-P15, both excitatory and inhibitory maps shrank along the isofrequency axis but expanded along the tonotopic axis. Along both axes, these changes were asymmetrical. Along the isofrequency axis, excitatory as well as inhibitory maps retracted exclusively along the VL direction (excitatory, $p < 0.001$, $n = 18$; inhibitory, $p < 0.05$, $n = 18$). Along the tonotopic axis, excitatory and inhibitory input areas expanded exclusively in the DL direction (excitatory, $p < 0.05$; $n = 18$; inhibitory, $p < 0.05$, $n = 18$) (Fig. 6*C*).

Between P13-P15 and P19-P22, both excitatory and inhibitory maps shrank along the tonotopic axis, in both the DL (excitatory, $p < 0.01$, $n = 20$; inhibitory, $p < 0.01$, $n = 20$) and VM (excitatory, $p < 0.05$, $n = 20$; inhibitory, $p < 0.05$, $n = 20$) directions (Fig. 6*C*). Very little refinement occurred along the isofrequency axis between P13-P15 and P19-P22, except that inhibitory maps shrank slightly along the DM direction ($p < 0.05$, $n = 20$, Student's *t* test) (Fig. 6*C*).

In summary, the sizes of excitatory and inhibitory synaptic input maps underwent two parallel alterations during the first two postnatal weeks. These changes were complex, yet spatially specific, and primarily involved a combination of growth and retraction along the isofrequency axis. During the first postnatal week, input maps expanded symmetrically along the isofrequency axis. During the second postnatal week, this growth was followed by a shrinkage of input maps that was restricted to the VL direction of the isofrequency axis, along which excitatory maps shrank relatively more than inhibitory maps. During the third postnatal week, map refinement was most dramatic and was primarily restricted to the VM and DL directions of the tonotopic axis resulting in excitatory maps that extended 80–320 μm (182 ± 100 μm, $n = 7$) and inhibitory maps that extended 160–360 μm (240 ± 83 μm, $n = 7$) along the tonotopic axis, which are comparable with the width of a fibrodendritic lamina in the IC (Shneiderman and Henkel, 1987; Malmierca et al., 1993; Fathke and Gabriele, 2009; Wallace et al., 2013).

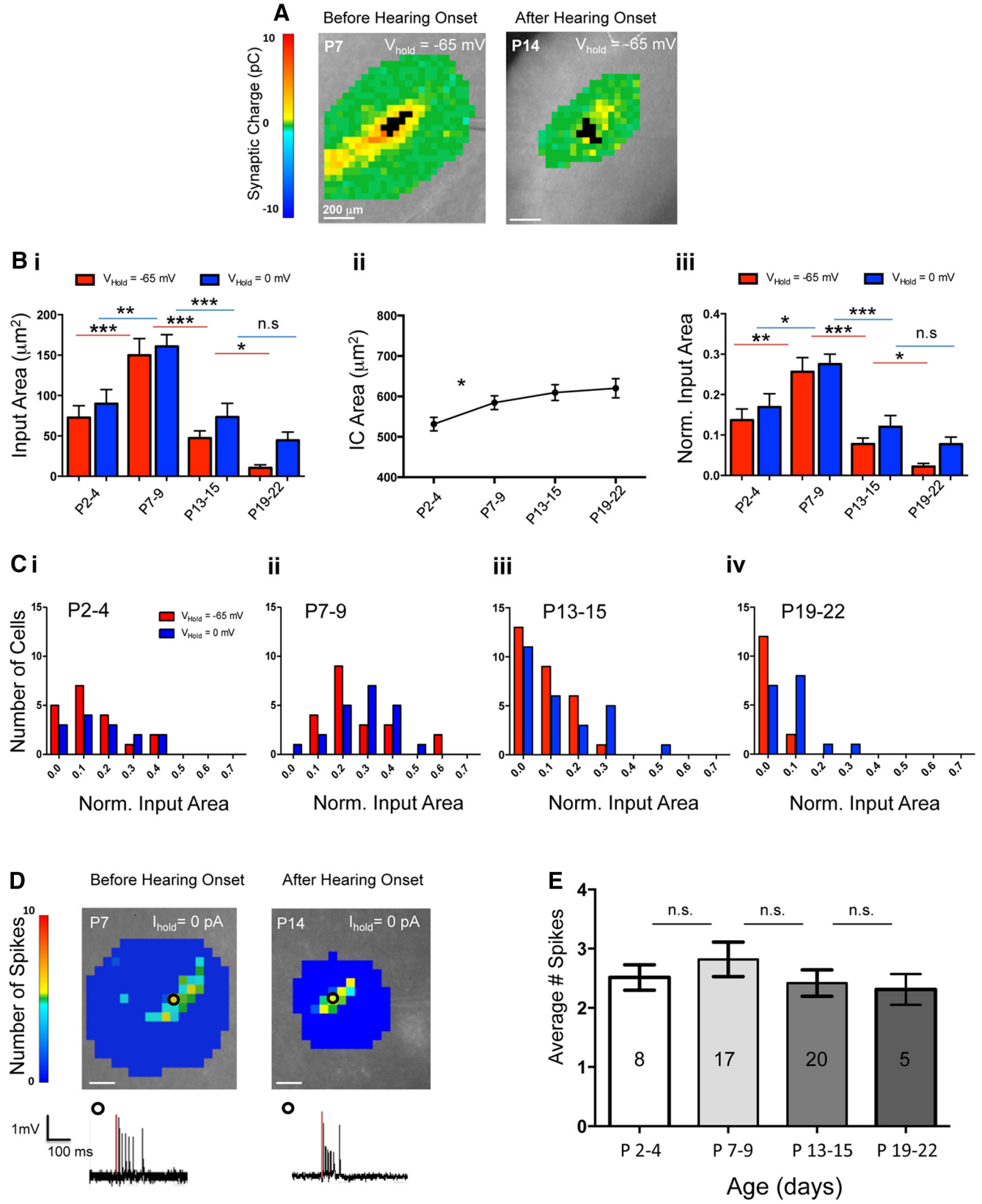

Figure 5. Developmental growth and refinement of local synaptic input maps. ***A***, Examples of synaptic input maps before (left) and after (right) hearing onset. ***B***, Age-dependent changes in the size of excitatory (red) and inhibitory (blue) synaptic input maps. ***Bi***, Absolute sizes of input maps at different ages. ***Bii***, Developmental increase of cross-sectional area of IC. ***Biii***, Synaptic input areas normalized to the cross-sectional are of the CNIC for each age group. *$p < 0.05$ (two-tailed t test). **$p < 0.01$ (two-tailed t test). ***$p < 0.001$ (two-tailed t test). n.s, Not significant ($p > 0.05$). ***C***, Distribution of excitatory and inhibitory synaptic input area sizes in each age group: P2-P4 (***i***), P7-P9 (***ii***), P13-P15 (***iii***), and P19-P22 (***iv***). ***D***, Neuronal excitability to glutamate uncaging during cell-attached recordings. Black circles represent stimulus locations from which example traces were recorded. Red line indicates UV light pulse. ***E***, The average number of spikes per stimulus was not significantly different between age groups. Numbers in bars indicate number of cells. Error bars indicate SEM.

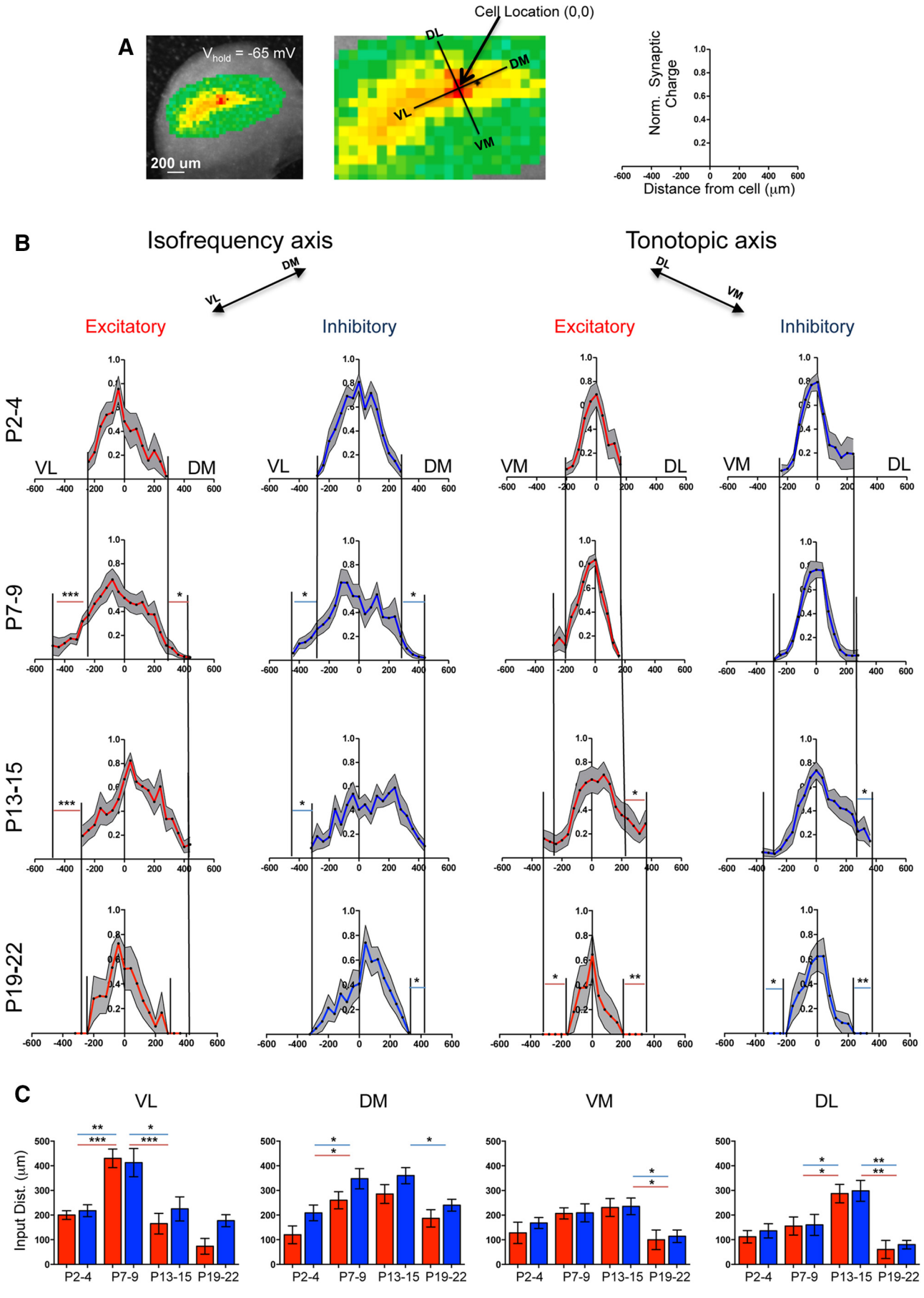
A
V_{hold} = -65 mV
200 um
Cell Location (0,0)
DL
DM
VL
VM
Norm. Synaptic Charge
Distance from cell (μm)
B
Isofrequency axis
Tonotopic axis
Excitatory
Inhibitory
P2-4
P7-9
P13-15
P19-22
C
Input Dist. (μm)

Relationship of excitatory and inhibitory input

To quantify the spatial relationship of excitatory and inhibitory intrinsic input maps in the developing CNIC, we first determined the spatial overlap of stimulation sites that elicited excitatory and inhibitory responses (Fig. 7). Overall, the amount of overlap between excitatory and inhibitory input maps was substantial (Fig. 7*C*,*D*), and there was no systematic shift in the locations of excitatory and inhibitory inputs relative to each other. Approximately 70% of stimulation sites that elicited excitatory responses also elicited inhibitory responses (E:I sites), and this percentage did not change with age (Fig. 7*C*). In contrast, the percentage of inhibitory stimulation sites that also elicited excitatory responses (I:E sites) was age dependent (Fig. 7*D*). At P2-P4, only 45% of sites that elicited inhibitory responses also elicited excitatory responses ($n = 15$ cells), indicating a dominance of GABAergic over glutamatergic intrinsic connectivity. During the first postnatal week, the I:E fraction increased to 66% at P7-P9 ($p < 0.01$, Mann–Whitney test, $n = 31$), indicating a relative increase of glutamatergic inputs. From P7-P9 to P13-P15, the I:E fraction significantly decreased again to 47% ($p < 0.05$, Mann–Whitney test, $n = 31$), indicating a shift back toward more inhibition at the time of hearing onset (Fig. 7*D*). This shift toward inhibition became more pronounced from P13-P15 to P19-P22 and the I:E fraction decreased to 31% ($p < 0.05$, Mann–Whitney test, $n = 30$). The fact that the I:E fraction decreased from P7-P9 to P13-P15, and from P13-P15 to P19-P22, but the E:I fraction remained constant, indicates that the sizes of excitatory maps decreased more than the sizes of inhibitory maps after hearing onset.

To quantify the magnitude of this difference, we calculated for each neuron the ratio of excitatory input area to inhibitory input area (E:I area index). Between P7-P9 and P13-P15, the mean E:I index decreased from 0.93 to 0.64, indicating that around the time of hearing onset, excitatory input area decreased by ~29%, relative to inhibitory input area ($p < 0.05$, Student's *t* test, $n = 31$) (Fig. 7*E*). Between P13-P15 and P19-P22, the mean E:I area index decreased from 0.64 to 0.32, indicating that, during the third postnatal week, excitatory input area decreased by ~32% relative to inhibitory area ($p < 0.05$, Student's *t* test, $n = 30$).

Although the size of an intrinsic input map illustrates the area in the CNIC from which neurons received synaptic inputs, it does not provide information about the amount of excitation or inhibition that IC neurons can receive from intrinsic sources. To address this question, we determined the total amount of excitation and inhibition received by each neuron by summing the synaptic charge from all stimulation sites. During the first postnatal week, the amount of synaptic excitation as well as inhibition dramatically increased, by approximately sixfold for excitation (from 34.8 pC to 209.8 pC, $n = 22$, $p < 0.01$) and fivefold for inhibition (from 78.9 pC to 385.6 pC, $n = 22$, $p < 0.01$) (Fig. 8*A*,*B*). Because the increase in the amounts of synaptic excitation and inhibition was similar, the mean E:I charge ratio remained unchanged (Fig. 8*C*). Between P7-P9 and P13-P15, the amount of excitation and inhibition decreased, but this decrease was not statistically significant (excitation, $p = 0.35$, Mann–Whitney test; inhibition, $p = 0.17$, Mann–Whitney test). However, the mean E:I ratio decreased by ~37%, from 0.61 to 0.38 ($p < 0.05$, Mann–Whitney test, $n = 31$) (Fig. 8*C*), indicating that total excitation decreased more than inhibition. Between P13-P15 and P19-P22, there was a dramatic decrease in the amount of excitation and inhibition, from 85.9 pC to 3.9 pC for excitation ($p < 0.05$, $n = 30$, Mann–Whitney test) and from 139.4 pC to 37.8 pC for inhibition ($p < 0.05$, $n = 30$, Mann–Whitney test). The magnitude of the changes in total strength of inhibition and excitation matched the magnitude of changes we observed in the size of excitatory and inhibitory input maps (Fig. 7*E*).

The dominance of local inhibition that emerged around hearing onset could result from a relative increase in inhibitory input area and/or from an increase in the strength of inhibitory connections. To address this question, we analyzed the charge density of excitatory and inhibitory maps (Fig. 8*D*,*E*). During the first postnatal week, charge density significantly increased for both excitatory and inhibitory maps ($p < 0.01$, $n = 22$ cells, two-tailed *t* test), indicating a strengthening of intrinsic connections during this developmental period. An increase in excitatory and inhibitory charge density was also observed during the second postnatal week, although this increase was not statistically significant (excitatory, $p = 0.54$; inhibitory, $p = 0.42$). The increase in excitatory and inhibitory strength was similar and as a result, the E:I charge density ratio remained the same (Fig. 8*F*).

During the third postnatal week, however, charge density decreased for both excitatory ($p < 0.01$, $n = 30$, Student's *t* test) and inhibitory connections ($p < 0.01$, $n = 30$, Student's *t* test) (Fig. 8*D*,*E*). This decrease was slightly greater for excitatory charge density then for inhibitory charge density, but the difference was not large enough to lead to a change in the E:I charge density ratio (Fig. 8*F*). In summary, these results indicate a dominance of GABAergic inhibition during the first three postnatal weeks, which increased in magnitude after hearing onset (Fig. 8*C*) because of a relative increase in inhibitory input area compared with excitatory input area.

Although excitatory and inhibitory inputs maps overlapped considerably, on a microcircuitry level, these maps could be heterogeneous, and individual presynaptic sites within these maps might be dominated by either excitation or inhibition. To address this possibility, we compared the strength of excitatory and inhibitory responses for each individual stimulation site from which both responses could be elicited (Fig. 9). In some neurons, the amplitudes of excitatory and inhibitory responses elicited from individual stimulation sites were highly correlated (linear correlation with slope approaching 1), whereas in other neurons, many stimulation sites gave rise to predominantly excitatory or inhibitory inputs (linear correlation with slope approaching 0) (Fig. 9*B*–*F*). In each age group, both the slopes and correlation coefficients were spread between 0 and 1. Negative correlations were rarely encountered, indicating that strong synaptic inputs of one type (either excitatory or inhibitory) were not systemically paired with weak inputs of the other type. Thus, the strengths of overlapping excitatory and inhibitory inputs were more likely to be balanced than antagonistic. Interestingly, in the neurons in which we observed a low correlation of excitatory and inhibitory response amplitudes, either excitation- or inhibition-dominated stimulation sites tended to cluster together (Fig. 9*F*), suggesting that these neurons receive spatially restricted "subclusters" of inputs that are predominately excitatory or inhibitory.

←

Figure 6. Refinement of input maps along the tonotopic and isofrequency axes. ***A***, Illustration of analysis. Excitatory and inhibitory synaptic inputs were calculated along each of four axes, relative to the location of the recorded neuron (VL, VM, DL, and DM). Right, Average excitatory and inhibitory synaptic charges (normalized to the maximum excitatory and inhibitory responses for that cell, respectively) are plotted as a function of distance from the recorded cell. ***B***, Excitatory (red) and inhibitory (blue) synaptic charges as a function of distance to the cell body along each of the four axes. Gray shaded areas represent ± SEM. Black lines indicate maximum extent of connections for each age group. ***C***, Average extent of excitatory and inhibitory synaptic input maps along each axis. Error bars indicate SEM. $^*p < 0.05$ (two-tailed *t* test). $^{**}p < 0.01$ (two-tailed *t* test). $^{***}p < 0.001$ (two-tailed *t* test).

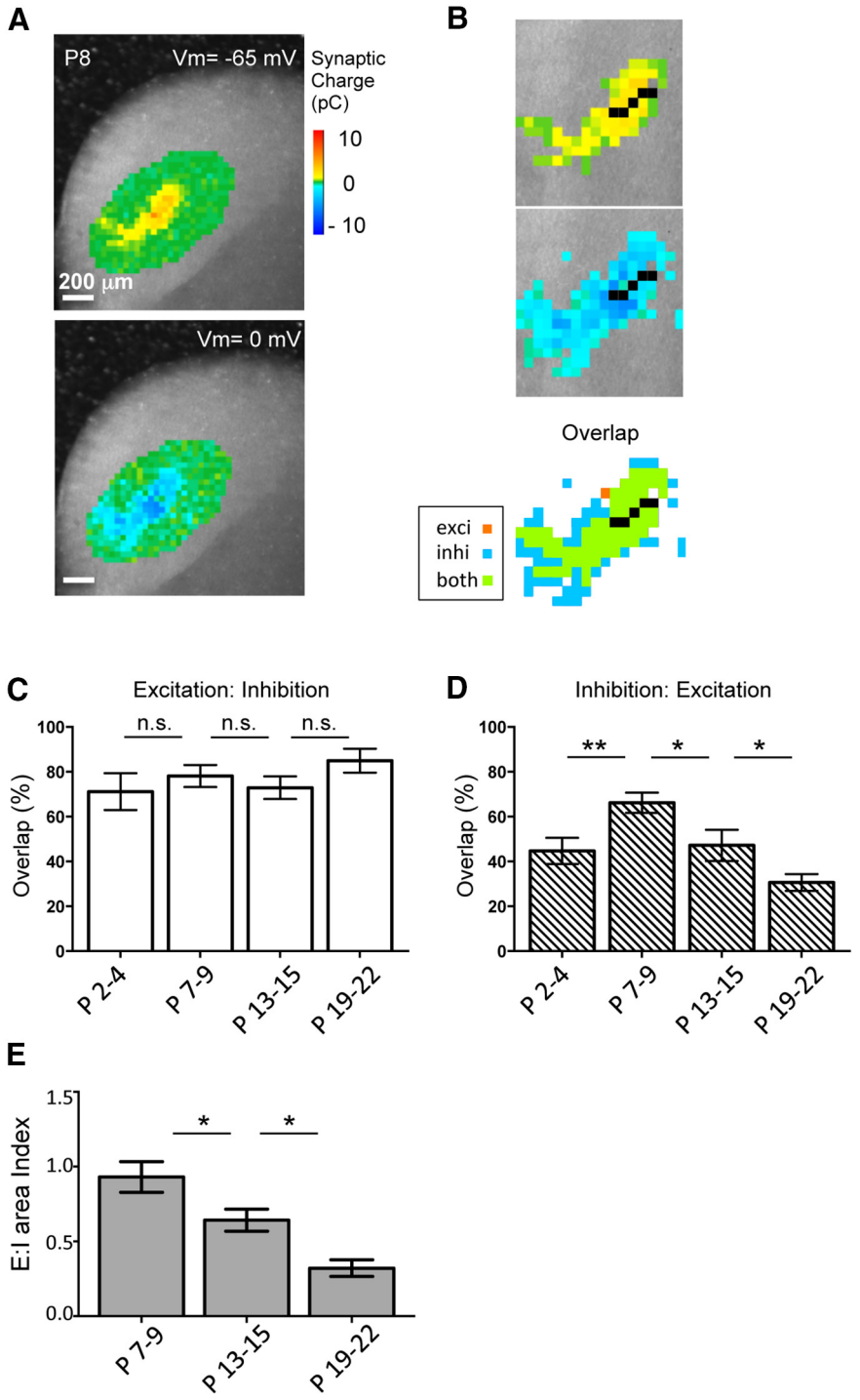

Figure 7. Spatial relationship of excitatory and inhibitory synaptic input maps. ***A***, Example excitatory (top) and inhibitory (bottom) input maps from a CNIC neuron (P7). Direct response areas are in black. ***B***, Same input maps at higher resolution. Bottom, Superimposition of excitatory and inhibitory synaptic maps. ***C***, Percentage of excitatory stimulation sites that also give rise to inhibitory responses: P2-P4, $n = 13$; P7-P9, $n = 18$; P13-P15, $n = 13$; P19-P22, $n = 12$. ***D***, Percentage of inhibitory stimulation sites that also give rise to excitatory responses. Same neurons as in ***C***.***E***, Mean ratios of area of excitation to area of inhibition for individual neurons: P7-P9, $n = 18$; P13-P15, $n = 13$; P19-P22, $n = 12$. Error bars indicate SEM. *$p < 0.05$ (two-tailed Student's *t* test). **$p < 0.01$ (two-tailed Student's *t* test). n.s., Not significant (two-tailed Student's *t* test).

Discussion

In this study, we used laser-scanning photostimulation with caged glutamate to provide the first characterization of functional intrinsic connectivity in the central nucleus of the inferior colliculus. Our results demonstrate that, already at P2, the CNIC contains an extensive excitatory and inhibitory intrinsic network. Excitatory and inhibitory inputs were spatially organized, forming continuous maps that largely overlapped with each other and that were aligned with the presumed isofrequency axis. This characteristic organization persisted throughout the first two postnatal weeks of development. However, the size of input maps was developmentally regulated undergoing an expansion during the first postnatal week that was followed by a significant shrinkage that began around the onset of hearing. These changes occurred in parallel for excitatory and inhibitory input maps, although the elimination of intrinsic connections was greater for excitatory than for inhibitory connections, resulting in a predominance of intrinsic inhibition at the end of the third postnatal week.

Technical considerations

An issue to consider when using photostimulation to map the organization of synaptic inputs is whether input maps represent monosynaptic or polysynaptic inputs. In our experiments, we aimed to stimulate monosynaptic inputs by using low concentrations of caged-glutamate (0.1 mM), low laser power (2 mW), and short laser pulse durations (1 ms). Our stimulation conditions were of significantly lower intensity than those used in other uncaging studies that activated monosynaptic connections in the auditory cortex and brainstem (Noh et al., 2010; Oviedo et al., 2010; Hirtz et al., 2012; Campagnola and Manis, 2014) but still yielded reliable input maps in the IC. Several lines of evidence argue in favor that our conditions primarily activated monosynaptic connections. First, disinhibiting the IC by blocking $GABA_A$ receptors, a condition that allows the recruitment of polysynaptic circuits (Sivaramakrishnan and Oliver, 2006; Chandrasekaran et al., 2013), did not affect excitatory input maps (Fig. 2). Second, the onset latencies of excitatory and inhibitory responses were indistinguishable (Fig. 3*C*,*D*), and both increased with distance from the recorded cell at similar rates of ~34 ms/mm (Fig. 3*B*). These rates are comparable with the rates reported for monosynaptic connections in the AVCN of adolescent mice recorded at slightly higher temperatures (Campagnola and Manis, 2014). Third, the average size of spike-eliciting areas obtained with cell-attached recordings was indistinguishable from the average size of direct stimulation areas obtained with whole-cell recordings in the presence of TTX (~400 μm^2), which blocks spike-elicited synaptic transmission. This indicates that presynaptic neurons activated under our photostimulation conditions

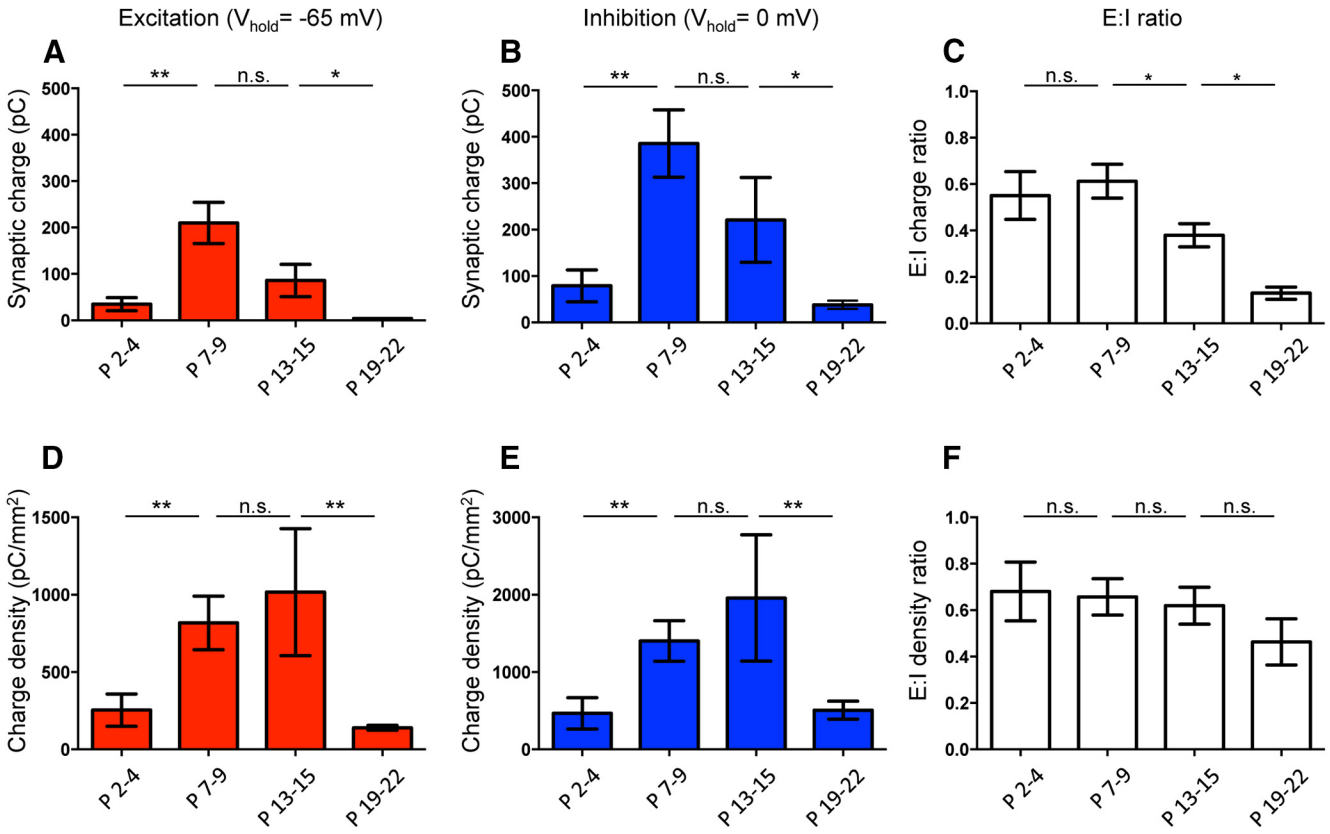

Figure 8. Development of the strength of intrinsic excitatory and inhibitory inputs. ***A***, Developmental changes of mean total excitatory synaptic charge received by CNIC neurons (mean ± SEM; P2-P4, $n = 9$; P7-P9, $n = 14$; P13-P15, $n = 10$; P19-P22, $n = 9$). ***B***, Mean total inhibitory synaptic charge received by same neurons as in ***A***. ***C***, Mean ratio of total excitatory and inhibitory synaptic charge per cell. ***D***, Developmental change of excitatory charge density (P2-P4, $n = 8$; P7-P9, $n = 14$; P13-P15, $n = 9$; P19-P22, $n = 11$). ***E***, Mean charge density of inhibitory maps (same neurons as in ***D***). ***F***, Ratio of excitatory charge density to inhibitory charge density at different ages. Error bars indicate SEM. *$p < 0.05$ (two-tailed Student's *t* test). **$p < 0.01$ (two-tailed Student's *t* test). ***$p < 0.001$ (two-tailed Student's *t* test). n.s., Not significant (two-tailed Student's *t* test).

do not elicit postsynaptic spikes that are necessary for polysynaptic transmission. Together, these results indicate that our input maps predominantly reflect the spatial organization of monosynaptic connections.

Organization of intrinsic synaptic input maps

Our studies demonstrate that functional, intrinsic input maps in the developing CNIC exhibit a laminar organization that closely follows the curvature of isofrequency contours in the CNIC (Ehret and Romand, 1994), thereby connecting neurons with similar best frequencies. This is consistent with previous anatomical (Oliver et al., 1991; Saldaña and Merchán, 1992; Malmierca et al., 1993, Miller et al., 2005; Wallace et al., 2012) and physiological (Grimsley et al., 2013) studies. Our results also revealed that this organization applies to both excitatory and inhibitory intrinsic circuits. The typical laminar organization was a consistent feature of all neurons that we recorded, despite the fact that our sample likely included many of the anatomically and physiologically distinct cell types that are present in the IC (Oliver and Morest, 1984; Peruzzi et al., 2000; Sivaramakrishnan and Oliver, 2001; Tan et al., 2007). Therefore, a laminar organization appears to be a fundamental feature of intrinsic connectivity that is shared by a wide variety of cell types in the IC.

Along the isofrequency domain, intrinsic input maps were continuous (e.g., not "patchy"), and the strength of both excitatory and inhibitory inputs diminished smoothly with increasing distance from the recorded neuron (Fig. 6). Thus, intrinsic connections can link different "functional zones," which share a common spectral tuning but receive different ascending (Aitkin and Schuck, 1985; Maffi and Aitkin, 1987; Shneiderman and Henkel, 1987; Oliver et al., 1997; Loftus et al., 2004; Malmierca et al., 2005; Cant and Benson, 2006) and/or descending inputs (Bajo and Moore, 2005). IC neurons in different functional zones exhibit distinct binaural response properties and periodicity preferences (Wenstrup et al., 1986; Schreiner and Langner, 1988; Loftus et al., 2010), and the integration of these elements by intrinsic IC circuits may facilitate the processing of complex acoustic features, such as tempo and rhythm (Bregman et al., 1985).

Along the tonotopic axis, excitatory and inhibitory input maps extended between 400 μm (P2-P4) and 600 μm (Fig. 5) at hearing onset. This indicates that, at this age, input maps likely span 2–6 frequency bands, or fibrodendritic lamina, each of which is ~100–200 μm wide (Shneiderman and Henkel, 1987; Malmierca et al., 1993; Fathke and Gabriele, 2009; Wallace et al., 2013). Wide input maps connecting several frequency bands may contribute to the immature frequency filters that are present at this age (Yu et al., 2005). Since the organization of ascending inputs to the IC is mature at hearing onset (Gabriele et al., 2000a, 2007; Henkel et al., 2007), the maturation of frequency filters that occurs after hearing onset (Ehret and Romand, 1994; Yu et al., 2005) may reflect the refinement of intrinsic IC maps that also occurs after hearing onset (Figs. 5 and 6).

Although in 3-week-old animals the average tonotopic width of intrinsic maps corresponded to the width of fibrodendritic laminae, ~30%–40% of maps (6 of 14) extended significantly >200 μm along the tonotopic axis (up to 400 μm), thus connect-

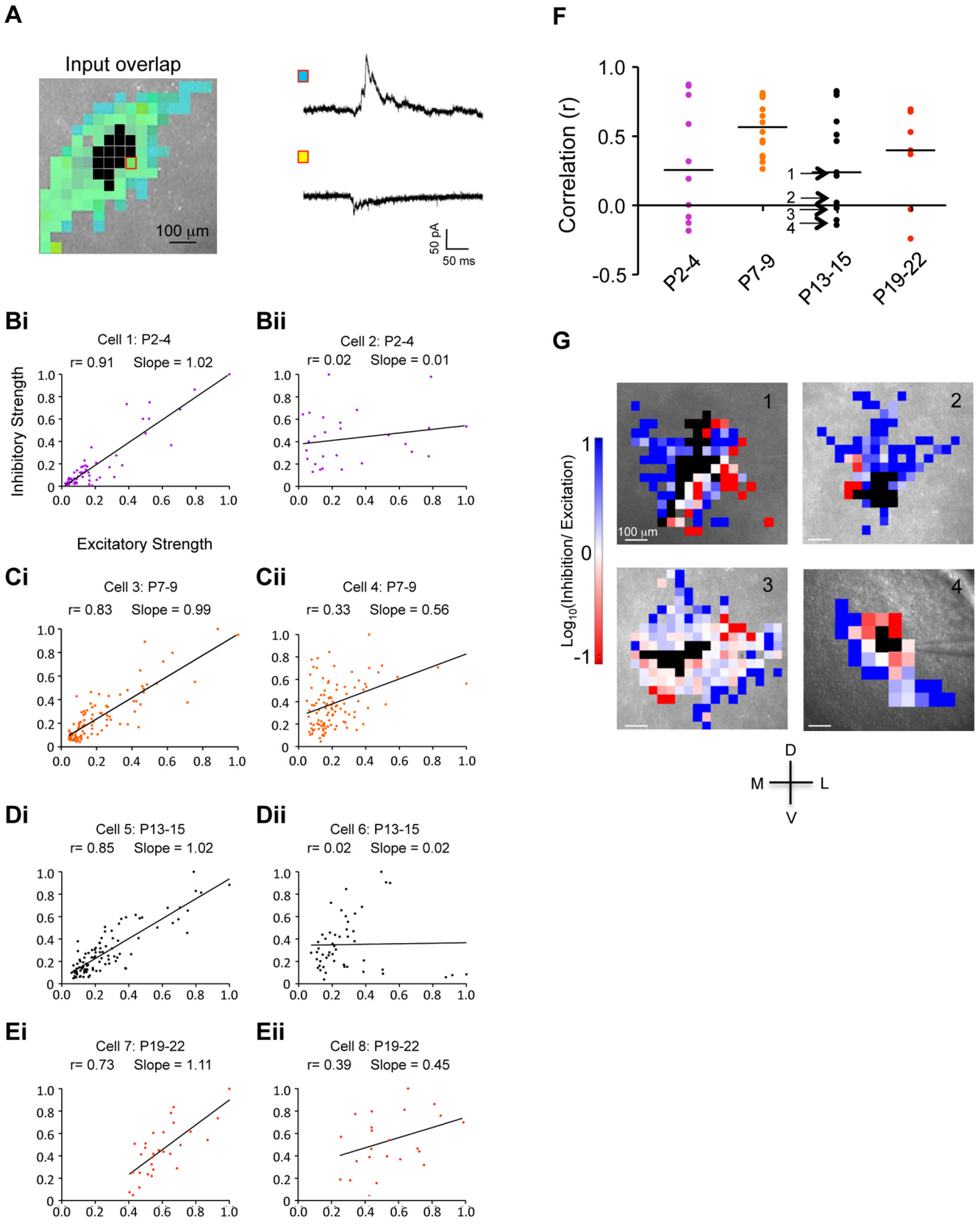

Figure 9. Relative synaptic strength of excitatory and inhibitory responses emanating from individual stimulation sites. ***A***, Example of superimposed excitatory and inhibitory inputs. Red box represents stimulation site that elicited the isolated excitatory and inhibitory responses shown to the right (blue represents inhibitory; yellow represents excitatory). Black boxes represent stimulation sites that elicited direct responses. ***B–E***, Excitatory versus inhibitory synaptic charge from corresponding stimulation sites, normalized to the peak charge. Two example neurons from each age group are shown (***i***, ***ii***). Each data point represents a single stimulation site. Lines indicate least-squares linear regressions and Pearson correlation coefficients (r). ***F***, Population of correlation coefficients. Horizontal black lines indicate median. ***G***, Input maps from four cells around hearing onset with r values ~0 (marked by arrows in ***E***). Stimulation sites dominated by inhibition or excitation are clumped together, but the pattern varies highly between cells.

ing 2–3 frequency bands. These tonotopically wide maps across could contribute to the broad tuning of subthreshold synaptic inputs (Xie et al., 2007) that exists despite the strict tonotopic termination patterns of extrinsic inputs (Oliver, 2000; Malmierca et al., 2005; Cant and Benson, 2006). It could also provide a neuronal substrate for the spectral integration of complex sounds seen, for example, in "combination-sensitive" neurons (Portfors and Felix, 2005). In mice, >30% of IC neurons are combination-sensitive and exhibit either combination-sensitive facilitation or inhibition, where a neuron's response to a particular sound frequency is either increased (facilitation) or decreased (inhibition) by the presence of a second sound that is separated by at least an octave (~3 frequency bands) (Portfors and Felix, 2005). Combination-sensitive facilitation and inhibition are important for creating selective responses to species-specific sounds in the IC (Klug et al., 2002), and the organization of intrinsic CNIC circuits is suitable to contribute to the generation of these responses. Because intrinsic circuits are preferentially engaged at higher sound intensities (Grimsley et al., 2013), intensity-dependent recruitment of excitatory and inhibitory intrinsic inputs from other fibrodendritic lamina may underlie the generation of the complex spectrotemporal receptive fields of CNIC neurons observed at higher sound intensities (Lesica and Grothe, 2008).

Intrinsic excitation: inhibition balance

Intrinsic excitatory and inhibitory synaptic input maps overlapped considerably during the first 3 postnatal weeks. However, after hearing onset, overlapping intrinsic excitatory and inhibitory inputs may be differentially engaged by different acoustic stimuli. For example, frequency response bandwidths in the IC broaden with increasing sound intensity (Egorova et al., 2001; Egorova and Ehret, 2008); and because extrinsic excitatory and inhibitory inputs to the CNIC saturate at higher sound levels (Grimsley et al., 2013), this broadening of tuning may be partly mediated by the recruitment of intrinsic excitatory circuits.

Although most presynaptic sites gave rise to both excitatory and inhibitory inputs, the correlation of the strength of excitation and inhibition arising from individual presynaptic sites varied widely between neurons (Fig. 9). At each age, we found neurons in which the strength of excitation and inhibition was remarkably correlated, suggesting that the strength of both inputs was adjusted in a coordinated manner. In other neurons, however, the correlation was basically absent, suggesting that, in these neurons, the strength of excitatory and inhibitory inputs is adjusted independently from each other (Fig. 9). Interestingly, in these neurons, stimulation sites that were dominated by either excitation or inhibition clustered together, giving rise to subinput maps, the organization of which varied considerably between neurons (Fig. 9). This heterogeneity on the microcircuit level adds to the large degree of heterogeneity of IC neurons observed in other studies (Peruzzi et al., 2000; Sivaramakrishnan and Oliver, 2001; Tan et al., 2007, Xie et al., 2007) and supports the idea that intrinsic excitatory and inhibitory microcircuits contribute to the generation of response preferences for specific frequency-temporal patterns of sound stimuli in individual IC neurons.

Developmental changes in intrinsic circuitry during the first 3 postnatal weeks

During the first postnatal week, both excitatory and inhibitory intrinsic synaptic input maps expanded along the isofrequency laminae (Figs. 5 and 6), and this expansion was accompanied by synaptic strengthening (Fig. 8*D*,*E*). During the same period, afferent projections from the DNLL segregate from a uniform to a banded termination pattern (Gabriele et al., 2000a; Henkel et al., 2005). This suggests that, during the first postnatal week, the development and refinement of extrinsic and intrinsic synaptic inputs in the CNIC are independently regulated. However, during the second postnatal week, when extrinsic inputs from the DNLL to the CNIC undergo refinement along the isofrequency domain, intrinsic input maps exhibited refinement along this domain as well. The prehearing refinement of these afferent projections to the CNIC requires cochlear-driven spontaneous activity (Gabriele et al., 2000b), and it remains to be determined whether similar mechanisms are necessary for the refinement of intrinsic input maps.

Although refinement of intrinsic input maps involved both excitatory and inhibitory connections, excitatory input maps shrank more than inhibitory input maps, such after 1 week of hearing a layer of inhibitory inputs surrounded excitatory input maps. The emergence of this surrounding inhibition may relate to the emergence of the inhibitory sidebands, which have been described in the IC of adult animals (Wang et al., 2002; Fuzessery et al., 2006). After hearing onset, map refinement was most dramatic and most pronounced for excitatory input along the tonotopic axis. The correlation of this refinement with hearing onset may indicate that tonotopic sharpening of excitatory intrinsic IC maps is triggered or guided by early auditory experience.

References

Adams JC (1979) Ascending projections to the inferior colliculus. J Comp Neurol 183:519–538. CrossRef Medline

Adams JC (1980) Crossed and descending projections to the inferior colliculus. Neurosci Lett 19:1–5. CrossRef Medline

Aitkin L, Schuck D (1985) Low frequency neurons in the lateral central nucleus of the cat inferior colliculus receive their input predominantly from the medial superior olive. Hearing Res 17:87–93. CrossRef Medline

Bajo VM, Moore DR (2005) Descending projections from the auditory cortex to the inferior colliculus in the gerbil, *Meriones unguiculatus*. J Comp Neurol 486:101–116. CrossRef Medline

Bregman AS, Abramson J, Doehring P, Darwin CJ (1985) Spectral integration based on common amplitude modulation. Percept Psychophys 37:483–493. CrossRef Medline

Brunso-Bechtold JK, Thompson GC, Masterton RB (1981) HRP study of the organization of auditory afferents ascending to central nucleus of inferior colliculus in cat. J Comp Neurol 197:705–722. CrossRef Medline

Burger RM, Pollak GD (2001) Reversible inactivation of the dorsal nucleus of the lateral lemniscus reveals its role for processing multiple sound sources in the inferior colliculus. J Neurosci 21:4830–4843. Medline

Campagnola L, Manis PB (2014) A map of functional synaptic connectivity in the mouse anteroventral cochlear nucleus. J Neurosci 34:2214–2230. CrossRef Medline

Cant NB, Benson CG (2006) Organization of the inferior colliculus of the gerbil (*Meriones unguiculatus*): differences in distribution of projections from the cochlear nuclei and the superior olivary complex. J Comp Neurol 495:511–528. CrossRef Medline

Cant NB, Benson CG (2008) Organization of the inferior colliculus of the gerbil (*Meriones unguiculatus*): projections from the cochlear nucleus. Neuroscience 154:206–217. CrossRef Medline

Casseday JH, Fremouw T, Covey E (2002) The inferior colliculus: a hub for the central auditory system. In: Integrative functions in the mammalian auditory pathway, pp 238–318. New York: Springer.

Chandrasekaran L, Xiao Y, Sivaramakrishnan S (2013) Functional architecture of the inferior colliculus revealed with voltage-sensitive dyes. Front Neural Circuits 7:41. CrossRef Medline

Egorova M, Ehret G (2008) Tonotopy and inhibition in the midbrain inferior colliculus shape spectral resolution of sounds in neural critical bands. Eur J Neurosci 28:675–692. CrossRef Medline

Egorova M, Ehret G, Vartanian I, Esser KH (2001) Frequency response areas of neurons in the mouse inferior colliculus: I. Threshold and tuning characteristics. Exp Brain Res 140:145–161. CrossRef Medline

Ehret G, Romand R (1994) Development of tonotopy in the inferior collicu-

lus II: 2-DG measurements in the kitten. J Neurosci 6:1589–1595. CrossRef Medline

Faingold CL, Anderson CA, Randall ME (1993) Stimulation or blockade of the dorsal nucleus of the lateral lemniscus alters binaural and tonic inhibition in contralateral inferior colliculus neurons. Hearing Res 69:98–106. CrossRef Medline

Fathke RL, Gabriele ML (2009) Patterning of multiple layered projections to the auditory midbrain prior to experience. Hearing Res 249:36–43. CrossRef Medline

Fuzessery ZM, Richardson MD, Coburn MS (2006) Neural mechanisms underlying selectivity for the rate and direction of frequency-modulated sweeps in the inferior colliculus of the pallid bat. J Neurophysiol 96:1320–1336. CrossRef Medline

Gabriele ML, Brunso-Bechtold JK, Henkel CK (2000a) Development of afferent patterns in the inferior colliculus of the rat: projection from the dorsal nucleus of the lateral lemniscus. J Comp Neurol 416:368–382. CrossRef Medline

Gabriele ML, Brunso-Bechtold JK, Henkel CK (2000b) Plasticity in the development of afferent patterns in the inferior colliculus of the rat after unilateral cochlear ablation. J Neurosci 20:6939–6949. Medline

Gabriele ML, Shahmoradian SH, French CC, Henkel CK, McHaffie JG (2007) Early segregation of layered projections from the lateral superior olivary nucleus to the central nucleus of the inferior colliculus in the neonatal cat. Brain Res 1173:66–77. CrossRef Medline

Grimsley CA, Sanchez JT, Sivaramakrishnan S (2013) Midbrain local circuits shape sound intensity codes. Front Neural Circuits 7:174. CrossRef Medline

Henkel CK, Gabriele ML, McHaffie JG (2005) Quantitative assessment of developing afferent patterns in the cat inferior colliculus revealed with calbindin immunohistochemistry and tract tracing methods. Neuroscience 136:945–955. CrossRef Medline

Henkel CK, Keiger CJ, Franklin SR, Brunso-Bechtold JK (2007) Development of banded afferent compartments in the inferior colliculus before onset of hearing in ferrets. Neuroscience 146:225–235. CrossRef Medline

Hirtz JJ, Braun N, Griesemer D, Hannes C, Janz K, Lohrke S, Muller B, Friauf E (2012) Synaptic refinement of an inhibitory topographic map in the auditory brainstem requires functional CaV1.3 calcium channels. J Neurosci 42:14602–14616. CrossRef Medline

Ito T, Bishop DC, Oliver DL (2009) Two classes of GABAergic neurons in the inferior colliculus. J Neurosci 29:13860–13869. CrossRef Medline

Kim G, Kandler K (2003) Elimination and strengthening of glycinergic/GABAergic connections during tonotopic map formation. Nat Neurosci 6:282–290. CrossRef Medline

Klug A, Bauer EE, Hanson JT, Hurley L, Meitzen J, Pollak GD (2002) Response selectivity for species-specific calls in the inferior colliculus of Mexican free-tailed bats is generated by inhibition. J Neurophysiol 88:1941–1954. Medline

Lesica NA, Grothe B (2008) Efficient temporal processing of naturalistic sounds. PLoS One 3:e1655. CrossRef Medline

Loftus WC, Bishop DC, Saint Marie RL, Oliver DL (2004) Organization of binaural excitatory and inhibitory inputs to the inferior colliculus from the superior olive. J Comp Neurol 472:330–344. CrossRef Medline

Loftus WC, Bishop DC, Oliver DL (2010) Differential patterns of inputs create functional zones in central nucleus of inferior colliculus. J Neurosci 30:13396–13408. CrossRef Medline

Maffi CL, Aitkin LM (1987) Differential neural projections to regions of the inferior colliculus of the cat responsive to high frequency sounds. Hearing Res 26:211–219. CrossRef Medline

Maling DH (1993) Coordinate systems and map projections, Ed 2. Amsterdam: Elsevier.

Malmierca MS (2004) The inferior colliculus: a center for convergence of ascending and descending auditory information. Neuroembryol Aging 5:215–229. DOI: 10.1159/000096799.

Malmierca MS, Blackstad TW, Osen KK, Karagülle T, Molowny RL (1993) The central nucleus of the inferior colliculus in rat: a Golgi and computer reconstruction study of neuronal and laminar structure. J Comp Neurol 333:1–27. CrossRef Medline

Malmierca MS, Merchán MA, Henkel CK, Oliver DL (2002) Direct projections from cochlear nuclear complex to auditory thalamus in the rat. J Neurosci 22:10891–10897. Medline

Malmierca MS, Saint Marie RL, Merchán MA, Oliver DL (2005) Laminar inputs from dorsal cochlear nucleus and ventral cochlear nucleus to the central nucleus of the inferior colliculus: two patterns of convergence. Neuroscience 136:883–894. CrossRef Medline

Malmierca MS, Izquierdo MA, Cristaudo S, Hernández O, Pérez-González D, Covey E, Oliver DL (2008) A discontinuous tonotopic organization in the inferior colliculus of the rat. J Neurosci 28:4767–4776. CrossRef Medline

Meininger V, Pol D, Derer P (1986) The inferior colliculus of the mouse: a Nissl and Golgi study. Neuroscience 17:1159–1179. CrossRef Medline

Merzenich MM, Reid MD (1974) Representation of the cochlea within the inferior colliculus of the cat. Brain Res 77:397–415. CrossRef Medline

Miller KE, Casseday JH, Covey E (2005) Relation between intrinsic connections and isofrequency contours in the inferior colliculus of the big brown bat, *Eptesicus fuscus*. Neuroscience 136:895–905. CrossRef Medline

Moore DR, Kotak VC, Sanes DH (1998) Commissural and lemniscal synaptic input to the gerbil inferior colliculus. J Neurophysiol 80:2229–2236. Medline

Morest DK, Oliver DL (1984) The Neuronal architecture of the inferior colliculus in the cat: defining the anatomy of the auditory midbrain. J Comp Neurol 222:209–236. CrossRef Medline

Noh J, Seal RP, Garver JA, Edwards RH, Kandler K (2010) Glutamate corelease at GABA/glycinergic synapses is crucial for the refinement of an inhibitory map. Nat Neurosci 13:232–238. CrossRef Medline

Oliver DL (1987) Projections to the inferior colliculus from the anteroventral cochlear nucleus in the cat: possible substrates for binaural interaction. J Comp Neurol 264:24–46. CrossRef Medline

Oliver DL (2000) Ascending efferent projections of the superior olivary complex. Microsc Res Tech 51:355–363. CrossRef Medline

Oliver DL (2005) Neuronal organization in the inferior colliculus. In: The inferior colliculus. New York: Springer.

Oliver DL, Morest DK (1984) The central nucleus of the inferior colliculus in the cat. J Comp Neurol 222:237–264. CrossRef Medline

Oliver DL, Kuwada S, Yin TC, Haberly LB, Henkel CK (1991) Dendritic and axonal morphology of HRP-injected neurons in the inferior colliculus of the cat. J Comp Neurol 303:75–100. CrossRef Medline

Oliver DL, Winer JA, Beckius GE, Saint Marie RL (1994) Morphology of GABAergic neurons in the inferior colliculus of the cat. J Comp Neurol 340:27–42. CrossRef Medline

Oliver DL, Beckius GE, Bishop DC, Kuwada S (1997) Simultaneous anterograde labeling of axonal layers from lateral superior olive and dorsal cochlear nucleus in the inferior colliculus of cat. J Comp Neurol 382:215–229. CrossRef Medline

Ono M, Yanagawa Y, Koyano K (2005) GABAergic neurons in inferior colliculus of the GAD67-GFP knock-in mouse: electrophysiological and morphological properties. Neurosci Res 51:475–492. CrossRef Medline

Oviedo HV, Bureau I, Svoboda K, Zador AM (2010) The functional asymmetry of auditory cortex is reflected in the organization of local cortical circuits. Nat Neurosci 13:1413–1420. CrossRef Medline

Peruzzi D, Sivaramakrishnan S, Oliver DL (2000) Identification of cell types in brain slices of the inferior colliculus. Neuroscience 101:403–416. CrossRef Medline

Pollak GD, Xie R, Gittelman J, Andoni S, Li N (2011) The dominance of inhibition in the inferior colliculus. Hearing Res 274:27–39. CrossRef Medline

Portfors CV, Felix RA 2nd (2005) Spectral integration in the inferior colliculus of the CBA/CaJ mouse. Neuroscience 136:1159–1170. CrossRef Medline

Romand R, Ehret G (1990) Development of tonotopy in the inferior colliculus: I. Electrophysiological mapping in house mice. Dev Brain Res 54:221–234. CrossRef Medline

Saldaña E, Merchán MA (1992) Intrinsic and commissural connections of the rat inferior colliculus. J Comp Neurol 319:417–437. CrossRef Medline

Saldaña E, Merchán MA (2005) Intrinsic and commissural connections of the inferior colliculus. In: The inferior colliculus, p 705. New York: Springer.

Saldaña E, Feliciano M, Mugnaini E (1996) Distribution of descending projections from primary auditory neocortex to inferior colliculus mimics the topography of intracollicular projections. J Comp Neurol 371:15–40. CrossRef Medline

Shneiderman A, Henkel CK (1987) Banding of lateral superior olivary nucleus afferents in the inferior colliculus: a possible substrate for sensory integration. J Comp Neurol 266:519–534. CrossRef Medline

Schreiner CE, Langner G (1988) Periodicity coding in the inferior colliculus of the cat: II. Topographical organization. J Neurophysiol 60:1823–1840. Medline

Schreiner CE, Langner G (1997) Laminar fine structure of frequency

organization in auditory midbrain. Nature 388:383–386. CrossRef Medline

Sivaramakrishnan S, Oliver DL (2001) Distinct K currents result in physiologically distinct cell types in the inferior colliculus of the rat. J Neurosci 21:2861–2877. Medline

Sivaramakrishnan S, Oliver DL (2006) Neuronal responses to lemniscal stimulation in laminar brain slices of the inferior colliculus. J Assoc Res Otolaryngol 7:1–14. CrossRef Medline

Stiebler I, Ehret G (1985) Inferior colliculus of the house mouse: I. A quantitative study of tonotopic organization, frequency representation, and tone-threshold distribution. J Comp Neurol 238:65–76. CrossRef Medline

Tan ML, Theeuwes HP, Feenstra L, Borst JG (2007) Membrane properties and firing patterns of inferior colliculus neurons: an in vivo patch-clamp study in rodents. J Neurophysiol 98:443–453. CrossRef Medline

Wallace MM, Kavianpour SM, Gabriele ML (2013) Ephrin-B2 reverse signaling is required for topography but not pattern formation of lateral superior olivary inputs to the inferior colliculus. J Comp Neurol 7:1585–1597. CrossRef Medline

Wallace MN, Shackleton TM, Palmer AR (2012) Morphological and physiological characteristics of laminar cells in the central nucleus of the inferior colliculus. Front Neural Circuits 6:55. CrossRef Medline

Wang J, Ding D, Salvi RJ (2002) Functional reorganization in chinchilla inferior colliculus associated with chronic and acute cochlear damage. Hearing Res 168:238–249. CrossRef Medline

Wenstrup JJ, Ross LS, Pollak GD (1986) Binaural response organization within a frequency-band representation of the inferior colliculus: implications for sound localization. J Neurosci 6:962–973. Medline

Willott JF, Shnerson A (1978) Rapid development of tuning characteristics of inferior colliculus neurons in mouse pups. Brain Res 148:230–233. CrossRef Medline

Winer JA, Larue DT, Diehl JJ, Hefti BJ (1998) Auditory cortical projections to the cat inferior colliculus. J Comp Neurol 400:147–174. CrossRef Medline

Xie R, Gittelman JX, Pollak GD (2007) Rethinking tuning: in vivo whole-cell recordings of the inferior colliculus in awake bats. J Neurosci 27:9469–9481. CrossRef Medline

Yu X, Wadghiri YZ, Sanes DH, Turnbull DH (2005) In vivo auditory brain mapping in mice with Mn-enhanced MRI. Nat Neurosci 8:961–968. CrossRef Medline